Desalination and Water Treatment
www.deswater.com

doi: 10.5004/dwt.2020.25475

187 (2020) 378–389
May

Adsorption of Congo red from solution by iron doped PVA-chitosan composite film

Kang Wen, Yi Li, Shuxing Zhang, Xiaoting Zhang, Runping Han*

College of Chemistry, Zhengzhou University, No 100 of Kexue Road, Zhengzhou 450001, China, Tel. +86 371 67781757; Fax +86 371 67781556; emails: rphan67@zzu.edu.cn (R. Han), 1039171416@qq.com (K. Wen), police78901@163.com (Y. Li), 1693444083@qq.com (S. Zhang), 1619888517@qq.com (X. Zhang)

Received 10 September 2019; Accepted 18 January 2020

ABSTRACT

Chitosan-polyvinyl alcohol-iron (CS-PVA-Fe) composite films with acid resistance and large adsorption capacity were prepared by doping trivalent iron, chitosan, and polyvinyl alcohol. The adsorption mechanism of Congo red (CR) on the composite films was investigated by changing the adsorption conditions (temperature, pH, salt) and characterization (isoelectric point, infrared spectroscopy, photoelectric spectroscopy, scanning electron microscopy). The results showed that the adsorption capacity of the composite film was 450 mg g^{-1} at pH 5.0, and the adsorption of CR by high concentration salt had only a slight negative effect. The adsorption was following Langmuir, pseudo-first-order kinetics and pseudo-second-order kinetics model, which showed that the adsorption process was based on the single-layer heterogeneous adsorption, and there were both physical and chemical adsorption processes. Thermodynamic analysis shows that adsorption was spontaneous, endothermic and entropy increasing process. According to the characterization analysis, the adsorption mechanism of CR was mainly hydrogen bonding, ion exchange, and complexation. Also, the desorption of CR-loaded film can be performed using 75% alcohol at pH 12. The results showed that CS-PVA-Fe composite films are promising as a suitable candidate for the efficient removal of CR from solution.

Keywords: Chitosan-polyvinyl alcohol-iron composite film; Congo red; Adsorption; Regeneration

1. Introduction

In modern times, enterprises mainly in the printing, dyeing industry, and paint industry have increased rapidly, which has led to the generation of a large amount of wastewater containing dyes [1–3]. Untreated effluents from these industries have a deleterious effect on the environment as well as on the health of people living within its catchment areas. These wastewater results in the increase of organic matter content, the change of chemical oxygen demand, and ultimately the death of organisms in water [4]. Dyes are known to contain nitro and amino compounds as well as some heavy metal elements such as copper, zinc, and arsenic. These pollutants enter the groundwater through water circulation and also have the potential of bioaccumulating in organisms which results in their increasing levels of toxicity [5–7]. Due to this issue associated with dyes, it is very important to treat dye-containing wastewater before it is released into the environment. Congo red (CR) as an anionic dye is applied in cotton, hemp, silk, leather, paper products dyeing as its structural stability and good dying effect. CR discharged into wastewater can cause serious damage to the environment. Besides, CR can be metabolized to benzidine, a known human carcinogen. So it is necessary to remove CR from the solution.

* Corresponding author.

At present, there are many treatment methods for wastewater containing dyes, which are usually divided into physical treatment, chemical treatment [8] and biological treatment and so on [9,10]. Among them, the adsorption technique has attracted wide attention because of its simple operation, mild reaction and low cost [11–13].

Chitosan (CS) is mainly prepared from chitin, a naturally occurring compound found in many fungal cell walls, nematodes, insect exoskeletons, and crustacean shells. The chemical structure of CS is a cationic polymer composed of alkaline polysaccharides [14]. Due to its large amount of amino acids and hydroxyl groups adjacent to amino groups, CS has chelating adsorption on many metal ions. It can also bind dyes and halogens through complexation and ion exchange. Thus, it can be used for the treatment of dye wastewater from industries (dye and food industries) to purify the environment and protect human health [15,16]. Chatterjee et al. [17] used multi walled carbon nanotubes impregnated chitosan to prepare hydrogel beads for removal of CR and chitosan modified carbon nanotube was effective to adsorb CR from solution. Chatterjee et al. [18] also studied CR adsorption on chitosan beads impregnated with cetyltrimethylammonium bromide and there was double the adsorption capacity. Du et al. [19] prepared graphene oxide/chitosan/silica fiber by wet spinning technology to adsorb CR, which proved that the adsorption effect was good.

Polyvinyl alcohol (PVA) is a water-soluble macromolecule material. Its main structure is 1,3-ethylene glycol. PVA can easily be used to form a film [20–22], and its mechanical properties are excellent. At the same time, PVA is the only vinyl polymer that can be used as a carbon source and energy by bacteria. Under certain conditions, it can be degraded naturally. The utility model belongs to a biodegradable environmentally-friendly macromolecule material.

Films materials are widely used in adsorption because of their large contact area and easy preparation [23,24]. The traditional CS film breaks down under weakly acidic conditions, which greatly limits its use in conditions with lower pH [25]. At the same time, the mechanical properties of single chitosan films are poor and easy to rupture in water [26]. Therefore, in this paper, trivalent iron, PVA, and CS were used to form a network structure to overcome the application range of single CS and increase its mechanical properties [27].

In this study, the aims are to prepare chitosan-polyvinyl alcohol-iron (CS-PVA-Fe) composite films (suitable in the weak acid environment) and study the adsorption property toward CR, based on characterization. The adsorption mechanism was discussed through various adsorption models, thermodynamic formulas and characterization.

2. Materials and methods

2.1. Material science

Ferric chloride ($FeCl_3·7H_2O$, Fengchuan Chemical Reagent, Tianjin, China), chitosan ($(C_6H_{11}NO_4)_n$·(CS), Chinese Pharmaceutical Chemical Reagent in Shanghai, China), polyvinyl alcohol ($[CH_2CH(OH)]_n$·(PVA), Fuchen Chemical Reagent, Tianjin, China), CR Dye (China Shanghai Aladdin Industrial Company), sodium hydroxide (NaOH, Fengchuan Chemical Reagent, Tianjin, China), glacial acetic acid (CH_3COOH, Fuyu Fine Chemical Industry, Tianjin, China), sodium sulfate (Na_2SO_4 The Third Chemical Plant, Jiaozuo, China), sodium nitrate ($NaNO_3$ Fengchuan Chemical Reagent, Tianjin, China) were all purchased. All working solutions were prepared by diluting the stock solution with an appropriate volume of distilled water. reagents were analytical grade.

2.2. Preparation of CS-PVA-Fe composite films

CS solution with a 3% mass fraction and PVA with a 4% mass fraction were mixed at a mass ratio of 2:1. The solution was mixed and then defoamed through the ultrasonic method. The mixed solution was added with 0.3 mol L^{-1} $FeCl_3$ solution, and the mass ratio of CS solution to trivalent iron solution was 3:1. After uniform mixing, a certain volume of mixed solution is added into the membrane casting device and put into the oven until the films are separated from the membrane casting device and then taken out. The films were soaked in NaOH solution for about 10 min and cleaned with deionized water. After neutralization, the films were spread out and dried in shade.

2.3. Characterization of CS-PVA-Fe composite films

The surface structure and composition of CS-PVA-Fe composite films were tested to analyze its adsorption mechanism. The point of zero charge (pH_{pzc}) of CS-PVA-Fe composite films was determined by adding 10 mg CS-PVA-Fe composite films to adjust the pH of sodium chloride solution with 0.1 mol L^{-1} mass concentration. Scanning electron microscopy (SEM, Hitachi S4800, Japan) was used to observe the surface morphology of the material at 1 kV voltage. Fourier transform infrared spectroscopy (FTIR, Nicolet IS50, USA) was applied to determine the change of characteristic functional groups of materials before and after adsorption. X-ray photoelectron spectroscopy (XPS, Escalab 250xi, England) was adopted to analyze CS-PVA-Fe composite films.

2.4. Adsorption experiments

The adsorption test of CS-PVA-Fe composite films toward CR was performed in batch mode. A certain amount of composite films and 10 mL solution of CR with a certain concentration were put into multiple conical flasks (50 mL), then shaken in a water bath with a certain temperature, 120 rpm lasting a certain time, respectively. The effects of adsorbent dosage (1–20 mg, C_0 = 500 mg L^{-1}, 303 K) and pH on adsorption (pH = 3–12) were investigated. The acidity and alkalinity of the solution were adjusted by 0.1 mol L^{-1} NaOH and 0.1 mol L^{-1} HCl solutions. The effects of salt concentration (0–0.35 mg L^{-1} $NaNO_3$, Na_2SO_4, C_0 = 500 mg L^{-1}, 303 K) and the influence of temperature on the adsorption of CR solution (293, 303, 313 K, 180 min) were performed.

After adsorption, the concentration of CR was determined and calculated using the spectrophotometer according to the standard curve of CR (at the maximum wavelength of 495 nm, 752, Shanghai Shun Yu Heng Ping Scientific Instruments Co. Ltd., China). The adsorption amount of

adsorbate (the amount of dyes adsorbed on adsorbent unit weight (q_e, mg g^{-1}) and the removal efficiency (P, %) were calculated by using the following Eqs. (1) and (2).

$$q = \frac{V\left(C_0 - C\right)}{m} \tag{1}$$

$$p = \frac{\left(C_0 - C\right)}{C_0} \times 100\% \tag{2}$$

where C_0 is the original dye concentration (mg L^{-1}), C shows the dye concentration (mg L^{-1}) at any time or equilibrium, V means the volume of the dye solution (L), m is the mass of CS-PVA-Fe composite films (g).

2.5. Desorption experiment

The spent CS-PVA-Fe composite films were obtained for CR adsorption at an initial concentration of 500 mg L^{-1} at 303 K. Then, CS-PVA-Fe films were washed with distilled water to remove the unadsorbed dye and dried at 333 K. The exhausted adsorbent was regenerated by alcohol 75% (pH = 12) solution. Repeat the above experiments several times. The regeneration yield was obtained as the ratio of values of q_e before and after regeneration.

3. Results and discussion

3.1. Characterization of composite films

3.1.1. SEM of CS-PVA composite films and CS-PVA-Fe composite films

The SEM image of CS-PVA composite films and CS-PVA-Fe composite films are recorded in Fig. 1. It is observed from Fig. 1a that there was smooth and complete, with no obvious impurities found on the surface of CS-PVA composite films. But there were a lot of wrinkles on the surface of CS-PVA-Fe composite films according to Fig. 1b, which broke the original tight and orderly structure of CS-PVA composite films. A similar phenomenon was found in the study of metal doping into chitosan composite films [28]. So the chemical reaction between Fe and CS had occurred, which might make the CS-PVA-Fe composite films stable in an acidic environment. Figs. 1c and d show the distribution of C, O and Fe on the composite films material and it was further seen that Fe had been successfully combined with the material.

3.1.2. FTIR analysis

In order to obtain the specific structure of the surface functional groups of CS-PVA-Fe composite films FTIR analysis is carried out and the results are shown in Fig. 2. It is seen from Fig. 2a that the strong peaks at 3,435 and 2,923 cm^{-1} from films were due to the stretching vibration of –OH or $–NH_2$ and the stretching vibration of C–H, respectively [29]. The peak at 1,638 cm^{-1} could be attributed to the C–N stretching vibration [30]. The peaks at 1,424 and 1,381 cm^{-1} were due to the bending vibration of C–H [31].

There was some change in absorption peaks after CR adsorption. The peaks at 3,435 and 2,923 cm^{-1} (N–H and C–H stretching vibration) became stronger and this proved that CR was successfully adsorbed with composite films. The characteristic peak of Fe–O was observed at 593 cm^{-1}, which proved that trivalent iron successfully binds to chitosan [32].

3.1.3. The pH of point zero charge

The pH of point zero charge (pH_{pzc}) indicates the electronic properties of surface functional groups in solution and it is helpful to judge the strong adsorption conditions. The results are shown in Fig. 3. It was seen that the pH_{pzc} value of CS-PVA-Fe was about 7.01. So there is a positive charge on the surface of CS-PVA-Fe composite films at the pH less than 7.01, this is favor of adsorption of CR (as anionic dyes), The pH of point zero charge of granular Fe-Zr-chitosan is about 7.0, which is similar to this study [33].

3.1.4. XPS analysis

The bonding mode between functional groups can explain the general structure and adsorption mechanism of materials [34,35]. Therefore, in order to explore the surface characteristics of CS-PVA-Fe composite films, XPS spectra of O 1s, Fe 2p and S 2p before and after CR adsorption are analyzed in Fig. 4. It is seen from Fig. 4 that the CS-PVA-Fe composite films mainly contain carbon, oxygen and nitrogen elements. The peak of S 2p (from CR structure) peak appeared after adsorption [36]. This result showed that CR was successfully adsorbed by the composite films. The groups on the surface of the film were further studied by XPS. Fig. 4b are spectra of sulfur after adsorption. The peak of S 2p in Fig. 4b represents the two combination modes of Fe–S–O under 169.1 eV and 168.7 ($–SO_3^{2-}$, $–SO^{2-}$) functional groups [37–39]. This indicated that there was an ion exchange between the negative group ($–SO_3^-$) on the surface of the adsorbent and the dye molecule.

3.2. Adsorption experiment

3.2.1. Effect of films dosage

The amount of adsorbent often determines the adsorption effect [40]. The proper amount of adsorbent was explored. CS-PVA-Fe composite films with different mass were added to 10 mL CR solution (500 mg L^{-1}) at 303 K for 3 h to study the effect of adsorbent dosage on adsorption, and the results are shown in Fig. 5. The results showed that the removal percent of CR increased from 19.6% to 98.2% with the increase of adsorbent dosage. With the increase of adsorbent dosage, the values of q_e decreased from 488.9 to 120.6 mg g^{-1}, because the adsorption capacity of CR per unit weight of adsorbent decreased with the increase of adsorbent mass, resulting in the decrease of q_e value. In the subsequent studies, 10 g L^{-1} adsorbent dose was selected.

3.2.2. Effects of solution pH

The pH of the solution has significant effects on the adsorbent and its chemical structure as well as the stability of the dye surface [41]. The state of CS-PVA-Fe composite films and CS-PVA composite films with the same mass in

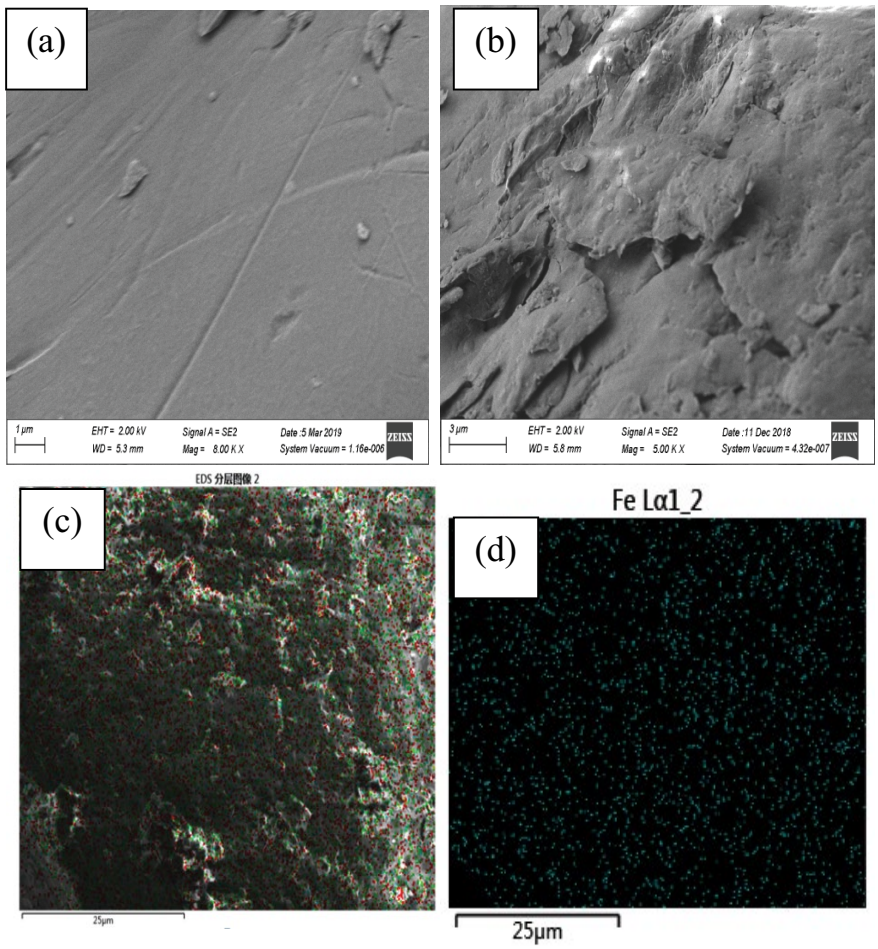

Fig. 1. SEM images of (a) CS-PVA, (b) CS-PVA-Fe, (c) CS-PVA-Fe mapping, and (d) Fe distribution.

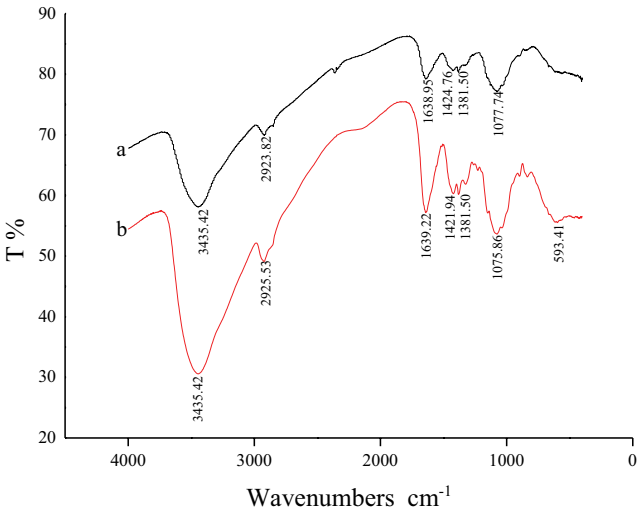

Fig. 2. FTIR of CS-PVA-Fe (a) and CR-loaded CS-PVA-Fe (b).

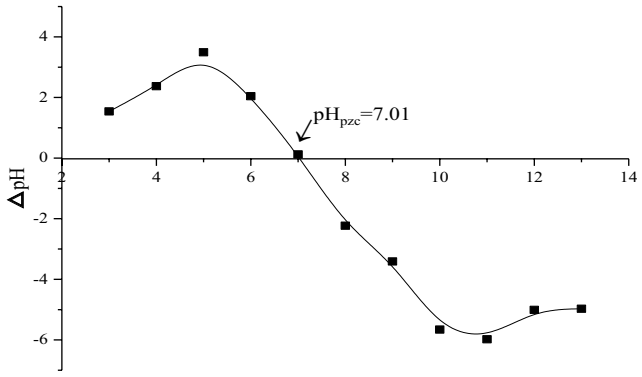

Fig. 3. The pH of point zero charge of CS-PVA-Fe.

CR solution at pH = 2 were compared after 3 h. As shown in Fig. 6, the color of CR solution will change from red to black in strongly acidic conditions. Because most of CR solution is adsorbed by CS-PVA-Fe composite films, the color of CR solution changed. At the same time, CS-PVA-Fe composite films (Fig. 6b) is slightly dissolved, but CS-PVA (Fig. 6d) has been nearly fully dissolved. Fig. 6a CS-PVA and Fig. 6c CS-PVA-Fe corresponds to uncut films in the original state). The values of q_e at different solution pH are shown in Fig. 7. It was observed that values of q_e increased rapidly under the acidic condition, but under alkaline conditions, q_e decreased slowly and then rapidly. The value of q_e at pH 5.0 was 450 mg g^{-1}. The amino group on the composite

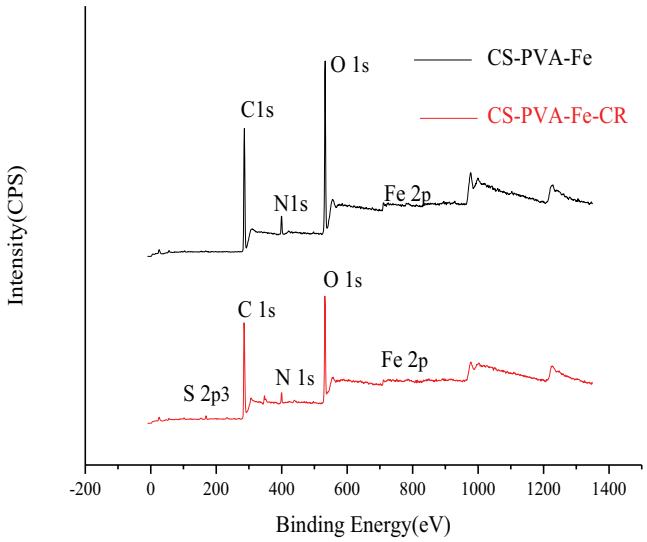

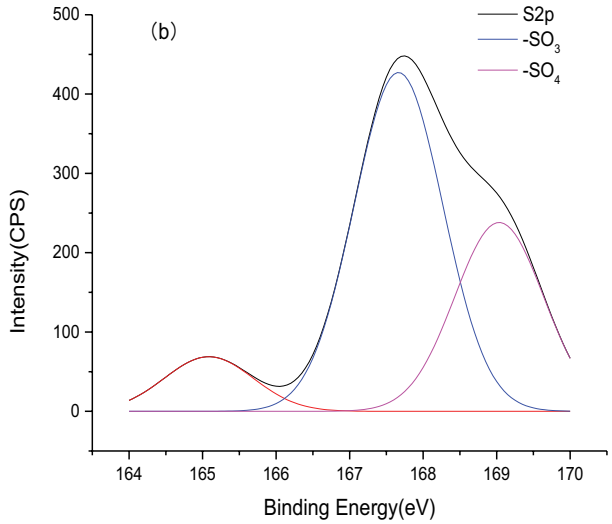

Fig. 4. XPS spectra of CS-PVA-Fe. (a) spectra of CS-PVA-Fe before and after CR adsorption and (b) S2p spectra after CR adsorption.

films was protonated at solution pH 5.0 and there was the electrostatic attraction between the composite film and CR. Similar results were recorded by CR adsorption on cationic surfactant modified wheat straw [42] and ethylenediamine modified wheat straw [43], 2,4-dichlorophenoxyacetic acid adsorption by Fe-crosslinked chitosan complex [44]. When the solution pH exceeded 7, the amino group was deprotonated. At the same time, a large number of OH^- and CR competed for the active sites on the surface of the composite films, which could make the adsorption amount decrease rapidly. Therefore, pH 5.0 is the best adsorption condition in this experiment.

3.2.3. The effect of salt concentration on adsorption

Industrial wastewater and domestic wastewater contain a large number of inorganic salt ions, which may have

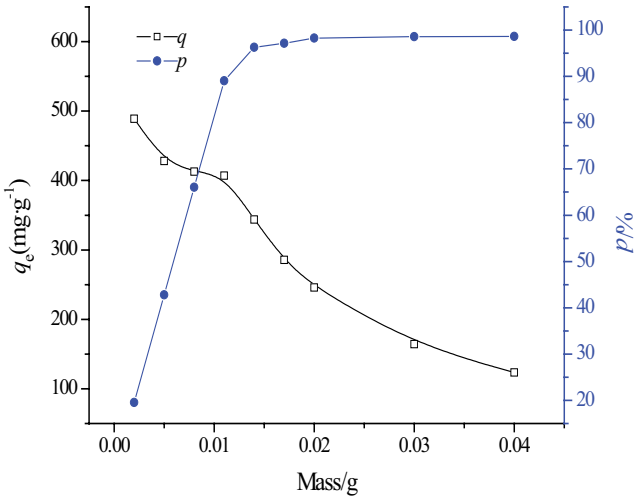

Fig. 5. Effect of adsorbent dose on CR adsorption.

a beneficial or adverse impact on the adsorption capacity. Therefore, it is necessary to determine the effect of ionic strength on dye adsorption [41]. The results at various salt concentrations are presented in Fig. 8. It is clear from Fig. 8 that the q_e value decreased with the increase of salt concentration, and there was more about the effect of Na_2SO_4. It was because the presence of inorganic salt ions in solution might shield the electrostatic interaction between the adsorbent and the opposite charge on the surface of the adsorbate, thereby reducing the adsorption capacity. But the trend of decrease was not significant as the value of q_e was from 446 to 422 mg g^{-1} at a salt concentration from 0 to 0.35 mol L^{-1}. So electrostatic attraction was not the main mechanism of interaction and there were other actions during the adsorption process. From the results obtained from the effect of salt and that of pH on the adsorption process, it could be inferred that complex action may be the major mechanism between CR and CS-PVA-Fe composite films.

3.2.4. Adsorption equilibrium study

The effect of CR concentration is performed and the results are displayed in Fig. 9. It was observed that the values of q_e became large with the increase of concentration and it was significant in favor of CR adsorption at higher temperatures. Therefore, it was concluded that the adsorption process be endothermic. Maybe the pores of the film became larger and this was an advantage of CR penetrating and resulted in higher adsorption capacity. The phenomenon of death like in the adsorption of CR by chitosan composite at 298–318 K was studied [45].

In this study, Langmuir model and Freundlich model were used to analyze the experimental data at 283, 293, 298, 303, and 313 K. Langmuir model assumes that the adsorbed molecule is a simple single-layer structure, all positions are energy-equivalent and there is no ideal state of interaction between the adsorbed molecules [46]. Freundlich model is a backward empirical formula suitable for describing heterogeneous surface adsorption of adsorbents. [47,48]. These two isotherm models can be expressed as:

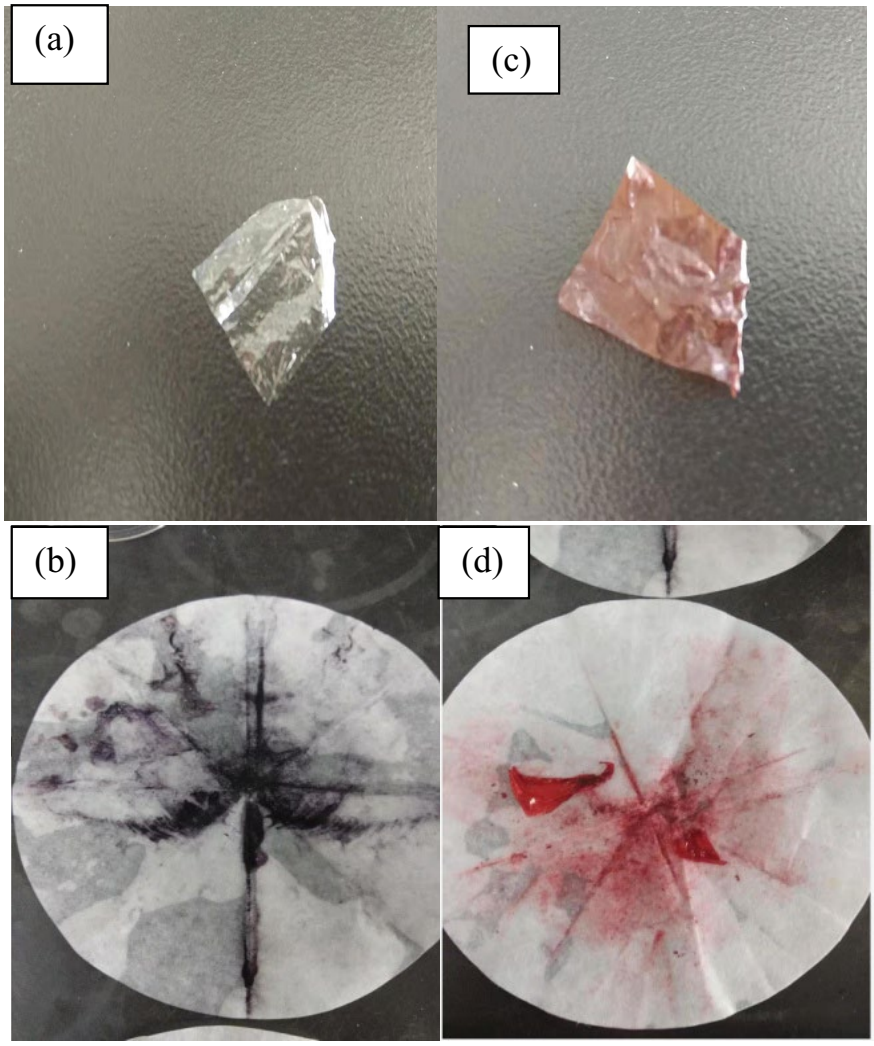

Fig. 6. The primitive state of CS-PVA (a) and CS-PVA-Fe (c); the states of CS-PVA (b) and CS-PVA-Fe (d) after CR adsorption at solution pH = 2.

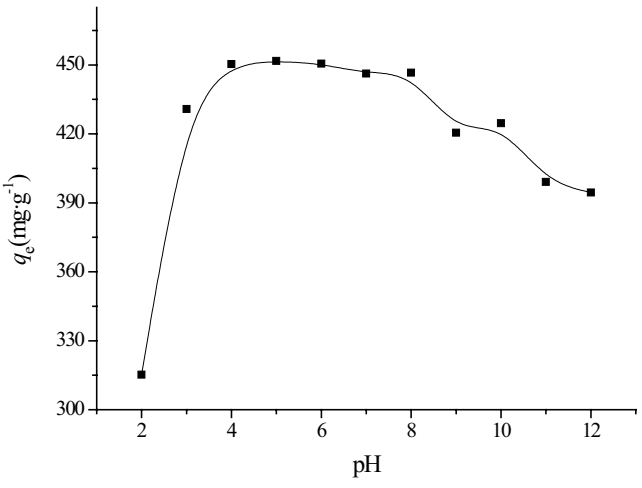

Fig. 7. Effect of pH on adsorption.

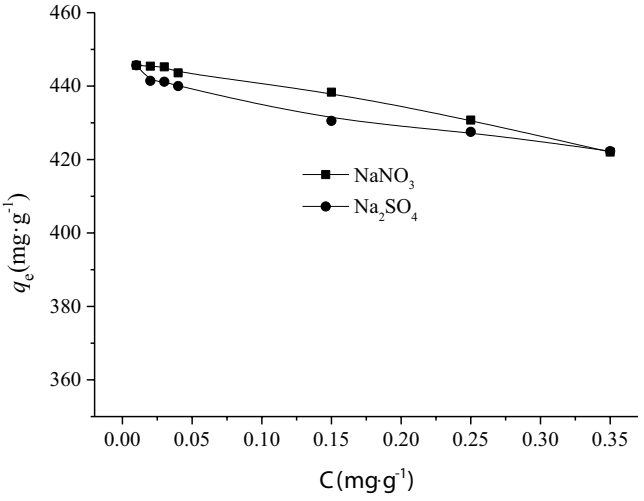

Fig. 8. Effect of salt concentration on adsorption.

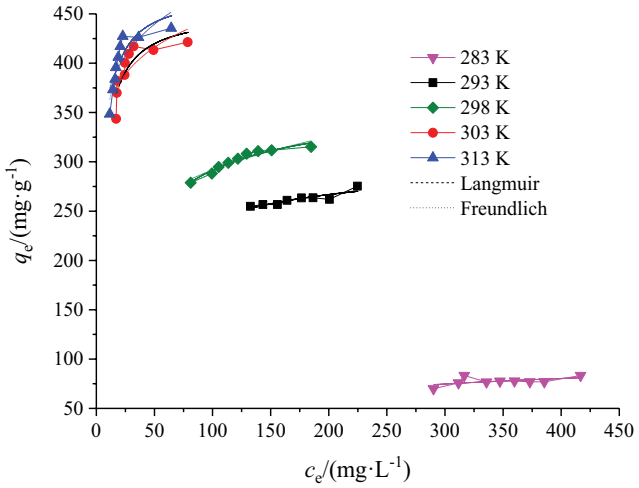

Fig. 9. Adsorption isotherms and fitting curves (CS-PVA-Fe).

The Eq. (3) of the Langmuir model:

$$q_e = \frac{q_m K_L C_e}{1 + K_L C_e} \tag{3}$$

Freundlich model:

$$q_e = K_F C_e^{1/n} \tag{4}$$

where q_m is the maximum adsorption capacity (mg g^{-1}), K_L denotes the affinity of binding sites and the correlation constant of adsorption energy (L mg^{-1}), K_F shows the Freundlich isotherm constant, $1/n$ represents the correlation constant of adsorption capacity and adsorption strength.

The nonlinear fitting parameters of the two models are recorded in Table 1 and the fitted curves are also shown in Fig. 9. Langmuir is more suitable for describing the adsorption process by numerical comparison (except at 293 K). There were bigger for both parameters from the Langmuir model at higher temperatures. The parameter of K_F increased with the increase of temperature, and the value of $1/n$ is below 0.2. This indicated very favorable conditions for the adsorption process.

3.2.5. Kinetic studies

The kinetic process is valuable to study and the results are presented in Fig. 10. It was observed from Fig. 10 that the values of q_t increased within 120 min and then maintained equilibrium. This phenomenon is due to the relatively large number of active sites on the adsorbent in the initial stage of adsorption, and the adsorption rate is faster; with the decrease of the active sites, the adsorption rate slows down. It was also found that adsorption quantity was enhanced at higher temperatures.

In order to further explore the adsorption mechanism of the composite films, the kinetic process was predicted by pseudo-first-order kinetic model, pseudo-second-order model, and Elovich equation. The pseudo-second-order model could be used to evaluate the mechanism of chemical adsorption [49–51]. Elovich equation was used to describe the heterogeneous adsorption of the ion exchange system [52]. The expressions of the three dynamic models are as follows.

Pseudo-first-order kinetic model:

$$q_t = q_e\left(1 - e^{-k_1 t}\right) \tag{5}$$

Pseudo-second-order kinetic model:

$$q_t = \frac{k_2 q_e^2 t}{1 + k_2 q_e t} \tag{6}$$

Elovich equation:

$$q_t = \frac{\ln(\alpha\beta)}{\beta} + \frac{\ln t}{\beta} \tag{7}$$

Table 1
CR isotherm model parameters

Langmuir model					
T/K	K_L/(L mg^{-1}) × 10^{-3}	$q_{m(exp)}$/(mg g^{-1})	$q_{m(theo)}$/(mg g^{-1})	R^2	SSE × 10^3
283	8.65 ± 6.7	83.3	104 ± 20	0.205	0.0905
293	41.1 ± 10	275	299 ± 9	0.741	0.0646
298	43.3 ± 4.2	315	359 ± 6	0.951	0.0505
303	259 ± 64	421	452 ± 15	0.722	1.27
313	286 ± 55	436	472 ± 14	0.824	1.03
Freundlich model					
T/K	K_F/(L mg^{-1})	$1/n$	R^2	SSE × 10^3	
283	18.1 ± 15	0.127 ± 0.025	0.200	0.0911	
293	193 ± 17	0.249 ± 0.14	0.780	0.0548	
298	142 ± 13	0.157 ± 0.018	0.901	0.101	
303	285 ± 27	0.0967 ± 0.028	0.571	1.97	
313	288 ± 25	0.108 ± 0.028	0.633	2.14	

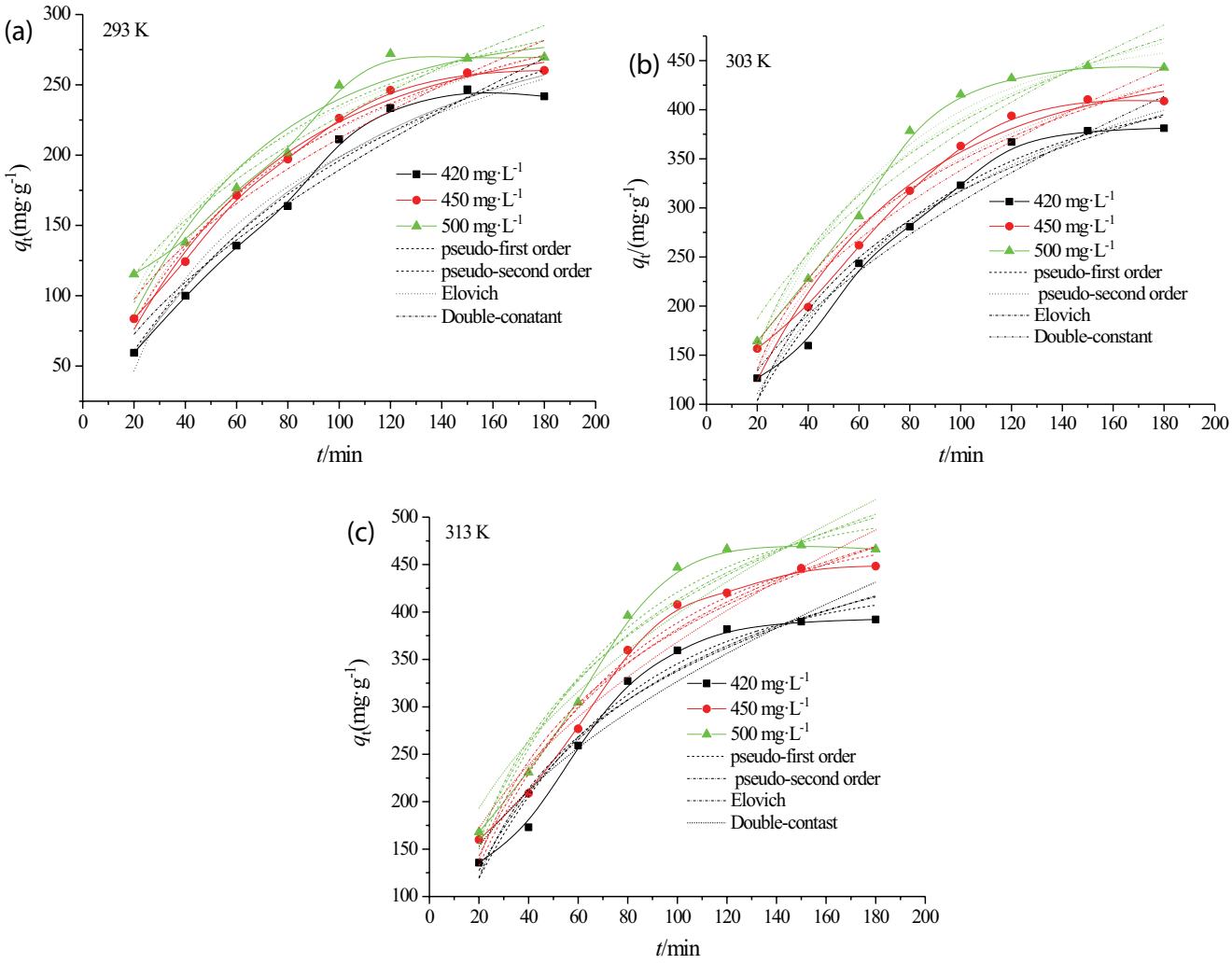

Fig. 10. Kinetic curves of CR adsorption at various concentrations and temperatures.

where q_t and q_e represents the adsorption quantity (mg g^{-1}) at time t and at equilibrium (mg g^{-1}); k_1 (min^{-1}) and k_2 (g mg^{-1} min^{-1}) are the rate constants of pseudo-first-order and pseudo-second-order kinetic models, respectively; α means the initial adsorption rate constant (mg g^{-1} min^{-1}) and the parameter β shows related to the extent of surface coverage and activation energy for chemisorption (g mg^{-1}).

The parameters of the dynamic model, $q_{e(theo)}$, the coefficient of determination (R^2) and the sum of squares of errors (SSE) are shown in Table 2 and the fitted curves at various conditions are also shown in Fig. 10. Pseudo-first-order equation and pseudo-second-order equation were suitable for this kind of adsorption as there were higher values of R^2 (0.9) and smaller values of SSE. Moreover, the fitted curves were closer to experimental curves at various conditions, respectively. Therefore, the pseudo-first-order kinetic model and pseudo-second-order model (rate-limiting steps, including hydrogen bonding or electron exchange between the composite films and CR) could well explain the adsorption mechanism. So there were physical and chemical effects in the adsorption process. At the same time, the Elovich equation could well describe the adsorption process and the adsorption process was also a process of ion exchange and heterogeneous diffusion [52].

3.2.6. Thermodynamic analysis

In order to further discuss the influence of temperature on the reaction and to determine whether the adsorption is endothermic or exothermic, the thermodynamic parameters including enthalpy (ΔH°), Gibbs free energy change (ΔG°) and entropy change (ΔS°) were determined using the following Eqs. (8)–(10) [53]:

$$K_c = \frac{C_{ad}}{C_e} \tag{8}$$

$$\Delta G^\circ = -RT \ln K_c \tag{9}$$

$$\Delta G^\circ = \Delta H^\circ - T\Delta S^\circ \tag{10}$$

$$\ln k_1 = -\frac{E_a}{RT} + \ln A \tag{11}$$

Table 2
Parameters of kinetic models for CR adsorption

Pseudo-first-order kinetic model						
T/K	C_0/(mg L^{-1})	$q_{e(exp)}$/(mg g^{-1})	$q_{e(theo)}$/(mg g^{-1})	k_1	R^2	SSE
293	420	245	299 ± 24	0.0109 ± 0.0017	0.971	859
	450	258	283 ± 7.2	0.0156 ± 0.0010	0.991	224
	500	270	288 ± 17	0.0178 ± 0.0029	0.922	1.84×10^3
303	420	380	428 ± 23	0.0140 ± 0.0017	0.972	1.62×10^3
	450	408	441 ± 19	0.0165 ± 0.0019	0.967	1.90×10^3
	500	440	476 ± 18	0.0182 ± 0.0019	0.970	2.09×10^3
313	420	390	430 ± 22	0.0162 ± 0.0021	0.964	2.21×10^3
	450	445	488 ± 23	0.0159 ± 0.0018	0.969	2.31×10^3
	500	470	511 ± 24	0.0173 ± 0.0022	0.961	3.33×10^3
Pseudo-second-order kinetic model						
T/K	C_0/(mg L^{-1})	$q_{e(exp)}$/(mg g^{-1})	$q_{e(theo)}$/(mg g^{-1})	k_2 (×10^{-5})	R^2	SSE × 10^3
293	420	245	441 ± 58	1.82 ± 0.3	0.964	1.09
	450	258	383 ± 19	3.52 ± 0.59	0.986	3.62
	500	270	373 ± 34	4.58 ± 0.15	0.927	1.74
303	420	380	592 ± 52	1.95 ± 0.54	0.967	1.93
	450	408	584 ± 40	2.57 ± 0.61	0.967	1.94
	500	440	623 ± 45	2.70 ± 0.70	0.958	2.99
313	420	390	580 ± 54	2.42 ± 0.77	0.95	3.11
	450	445	657 ± 52	2.12 ± 0.57	0.963	2.83
	500	470	678 ± 61	2.30 ± 0.73	0.944	4.75
Elovich equation						
T/K	C_0/(mg L^{-1})	α	β	R^2	SSE × 10^3	
293	420	–238 ± 35	94.7 ± 8.0	0.952	1.43	
	450	–189 ± 22	88.5 ± 4.9	0.979	0.549	
	500	–149 ± 41	83.0 ± 9.4	0.917	1.99	
303	420	–294 ± 49	133 ± 11	0.952	2.84	
	450	–259 ± 48	132 ± 11	0.954	2.65	
	500	–279 ± 58	145 ± 13	0.945	3.85	
313	420	–285 ± 58	135 ± 13	0.937	3.88	
	450	–310 ± 57	150 ± 13	0.945	3.83	
	500	–349 ± 71	158 ± 16	0.931	5.88	

where K_c is the coefficient of adsorption distribution, C_{ad} shows the concentration of CR on adsorbent at equilibrium (mg L^{-1}), R (8.314 J mol^{-1} K^{-1}) is the ideal gas constant, and T means the absolute temperature (K). E_a is the activation energy of Arrhenius adsorption, and A (g mg^{-1} min^{-1}) represents the temperature-dependent parameter factor.

The thermodynamic parameters calculated from the above equations are shown in Table 3. The value of $\Delta G°$ was negative, indicating that the adsorption was spontaneous. The positive value of $\Delta H°$ indicated that the reaction was endothermic. As the value of $\Delta H°$ was over 40 kJ mol^{-1}, the adsorbent had a strong binding force toward the adsorbate, including the chemical process [54]. At the same time, the positive value of $\Delta S°$ indicated that the entropy became larger and the degree of disorderliness increased during the adsorption process. E_a value was 142 kJ mol^{-1}, which indicated that there was chemical action in the adsorption process [55,56]. In summary, chemical reactions were dominant in the adsorption process. Thermodynamic parameters indicated that the adsorption was a spontaneous, endothermic and entropy-increasing reaction.

3.2.7. Desorption regeneration experiment

Whether the adsorbent can be reused many times is also an important basis for judging whether the adsorbent can be applied to actual adsorption [57–59]. So the regeneration and reuse of CR -loaded or spent CS-PVA-Fe composite films is necessary to be carried out. Medical alcohol with 75% volume fraction was adjusted to pH = 12 and used as eluent, and CR adsorbed on composite films was regenerated by three times. The desorption efficiency

was 57.6%, 62.2%, and 45.1% respectively. The regeneration efficiency of the three cycles were all above 50%. It can be concluded that an alkaline environment destroys the interaction between adsorbent and CR, and organic solvents accelerate the release of CR by using a similar compatibility principle. Analytical dynamics tests were carried out at 313 K. The results of nonlinear fitting of analytical dynamics were shown in Fig. 11. The determined coefficients of the Elovich equation and double constant equation R^2 were 0.920 and 0.956, and SSE values were 46.2 and 22.5, respectively. The results showed that there was ion exchange in the desorption process [52].

The adsorption capacity of various adsorbents toward CR was listed in Table 4. Compared with different adsorbents, the adsorption capacity of CS-PVA-Fe composite films toward CR is larger [17–19,60]. Furthermore, there was some property of desorption and reuse. So it is some advantage of CR adsorption from solution.

Table 3
Thermodynamic parameters of CR adsorption on Composite Film

E_a (kJ mol^{-1})	$\Delta H°$ (kJ mol^{-1})	$\Delta S°$ (kJ mol^{-1} K^{-1})	$\Delta G°$ (kJ mol^{-1})		
			293 K	303 K	313 K
142	101	0.354	–1.51	–7.57	–8.85

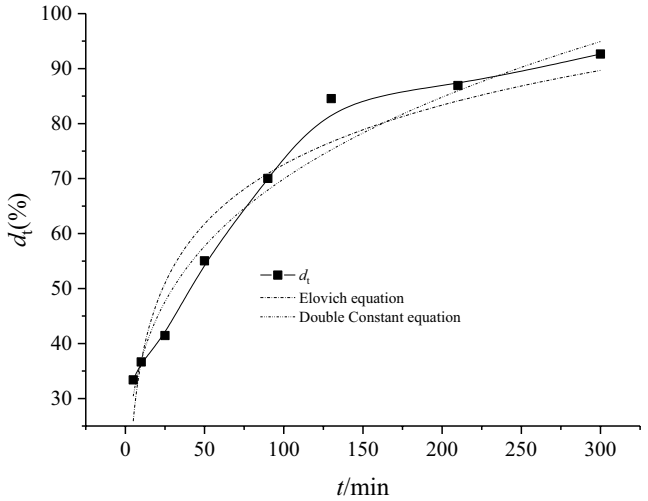

Fig. 11. Kinetics of CR desorption.

3.2.8. Adsorption mechanism of CS-PVA-Fe composite films

The functional groups of chitosan contain a large number of amino and hydroxyl groups. Adding iron at the same time could make polyvinyl alcohol chitosan form a network structure [27], which could interact with dye molecules. When adsorbed, the $–NH_2$ the surface of adsorbent was protonated to $–NH_3^+$, and the sulfonate group of dye was dissociated and transformed into anions. The electrostatic interaction between the two counter-ions forms a pair of ions. At the same time, sulfonate groups could be combined with iron through complexation, and N, S, O in CR molecule could

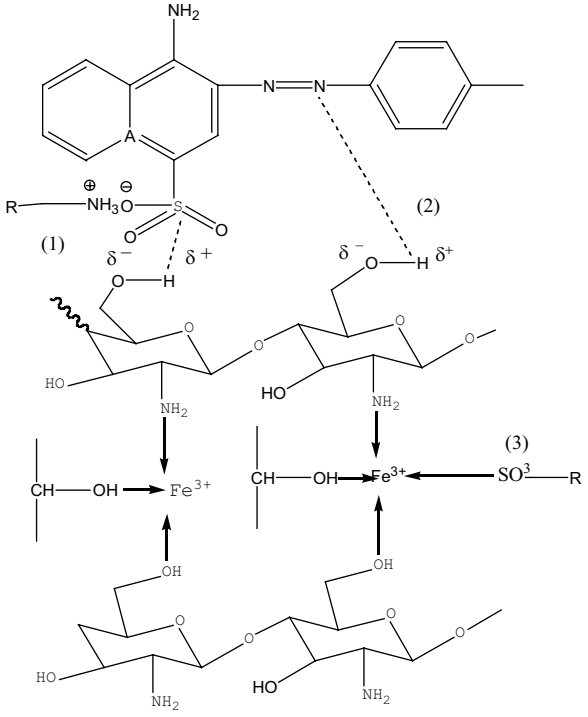

Fig. 12. Adsorption mechanism of CR on composite films.

Table 4
Comparison of adsorption capacity with various adsorbents CR

Adsorbents	Adsorption capacity (mg g^{-1})	Ref.
Chitosan beads impregnated with carbon nanotubes	400	[17]
Chitosan hydrogel beads impregnated with bromide	352	[18]
Graphene oxide/chitosan fibers	245	[19]
polyethyleneimine modified wheat straw	89.7	[31]
Ethylenediamine modified wheat straw	68.6	[43]
Chitosan coated magnetic Fe_3O_4 particle	56.7	[48]
Magnesium oxide (MgO)-graphene oxide	237	[60]
CS-PVA-Fe	425	Present study

also form hydrogen bonds with a film surface. Fig. 12 shows a diagram of the interaction of CS-PVA-Fe composite films and CR.

4. Conclusion

A new type of carbon-polyvinyl alcohol-iron composite film as adsorbent was successfully prepared. Through adsorption experiments, characterization and data fitting, the following conclusions were drawn: the new adsorbent had a good adsorption effect on CR; the film had a good adaptability to acidic conditions, and salt had a slight negative impact on adsorption. The kinetics of the adsorption process conforms to the pseudo-first-order kinetic model, pseudo-second-order model. The chemical effect was the main factor in the adsorption process. The adsorption process was spontaneous, endothermic and entropy-increasing. The new composite films had excellent adsorption capacity toward CR and there was promising to applied in the removal of CR from solution.

Acknowledgement

This work was financially supported by the Henan province basis and advancing technology research project (142300410224).

References

[1] K.B. Tan, M. Vakili, B.A. Horri, P.E. Poh, A.Z. Abdullah, B. Salamatinia, Adsorption of dyes by nanomaterials: recent developments and adsorption mechanisms, Sep. Purif. Technol., 150 (2015) 229–242.
[2] P.F. Wang, M.H. Cao, C. Wang, Y.H. Ao, J. Hou, J. Qian, Kinetics and thermodynamics of adsorption of methylene blue by a magnetic graphene–carbon nanotube composite, Appl. Surf. Sci., 290 (2014) 116–24.
[3] M. Iqbal, M. Abbas, Bioassays based on higher plants as excellent dosimeters for ecotoxicity monitoring: a review, Chem. Int., 5 (2019) 1–80.
[4] E.M. Seftel, R.G. Ciocarlan, B. Michielsen, V. Meynen, S. Mullens, P. Cool, Insights into phosphate adsorption behavior on structurally modified Zn-Al layered double hydroxides, Appl. Clay Sci., 165 (2018) 234–246.
[5] P. Bocher, F. Caurant, P. Miramand, Y. Cherel, P. Bustamante, Influence of the diet on the bioaccumulation of heavy metals in zooplankton–eating petrel at Kerguelenarchipelago, Southern Indian Ocean, Polar. Biol., 26 (2003) 759–756.
[6] A. Begum, M.N. Amin, S. Kaneco, K. Ohta, Selected elemental composition of the muscle tissue of three species of fish, Tilapia nilotica, Cirrhina mrigala, and Clarius batrachus, from the freshwater Dhanmondi Lake in Bangladesh, Food Chem., 93 (2005) 439–443.
[7] M. Iqbal, F. Vicia, Bioassay for environmental toxicity monitoring: a review, Chemosphere, 144 (2016) 785–802.
[8] I. Ciabatti, F. Tognotti, L. Lombardi, Treatment, and reuse of dyeing effluents by potassium ferrate, Desalination, 250 (2010) 222–228.
[9] S. Sinha, R. Singh, A.K. Chaurasia, S. Nigam, Self-sustainable *Chlorella pyrenoidosa* strain NCIM 2738 based photobioreactor for removal of Direct Red–31 dye along with other industrial pollutants to improve the water-quality, J. Hazard. Mater., 306 (2016) 386–394.
[10] K.C. Ahire, B.P. Kapadnis, G.J. Kulkarni, R.L. Deopurkar, Biodegradation of tributyl phosphate by novel bacteria isolated from enrichment cultures, Biodegradation, 23 (2012) 165–176.
[11] X. Xu, B.Y. Gao, B. Jin, Q.Y. Yue, Removal of anionic pollutants from liquids by biomass materials: a review, J. Mol. Liq., 215 (2016) 565–595.
[12] C. Obi, K. Robinson, Surface interaction of sweet potato peels (Ipomoea batata) with Cd (II) and Pb (II) ions in aqueous medium, Chem. Int., 4 (2018) 221–229.
[13] A. Ayach, S. Fakhi, Z. Faiz, A. Bouih, O. Ait malek, A. Benkdad, M. Benmansour, A. Laissaoui, M. Adjour, Y. Elbatal, I. Vioque, G. Manjon, Adsorption of Methylene Blue on bituminous schists from Tarfaya-Boujdour, Chem. Int., 3 (2017) 343–352.
[14] H. Harmoudi, L. Gaini, E. Daoudi, M. Rhazi, Y. Boughaleb, M.A. Mhammedi, Removal of 2,4–D from aqueous solutions by adsorption processes using two biopolymers: chitin and chitosan and their optical properties, Opt. Mater., 36 (2014) 1471–1477.
[15] B. Krajewska, Diffusion of metal ions through gel chitosan membranes, React. Funct. Polym., 47 (2001) 37–47.
[16] C. Chatelet, O. Damour, A. Domard. Influence of the degree of acetylation on some biological properties of chitosan. films, Biomaterials, 22 (2001) 261–268.
[17] S. Chatterjee, M.W. Lee, S.H. Woo, Adsorption of congo red by chitosan hydrogel beads impregnated with carbon nanotubes, Bioresour. Technol., 101 (2009) 1800–1806.
[18] S. Chatterjee, M.W. Lee, S.H. Woo, Enhanced adsorption of congo red from aqueous solutions by chitosan hydrogel beads impregnated with cetyltrimethyl ammonium bromide, Bioresour. Technol., 100 (2008) 2803–2809.
[19] Q.J. Du, J.K. Sun, Y.H. Li, Highly enhanced adsorption of congo red onto graphene oxide/chitosan fibers by wet-chemical etching off silica nanoparticles, Chem. Eng. J., 245 (2014) 99–106.
[20] M. Tsukada, G. Freddi, S. John, Structure and compatibility of poly (vinyl al–coho1) silk fibroin (PVA/SA) blend films, J. Polym. Sci., 32 (2010) 243–248.
[21] C. Liu, R. Bai, Adsorptive removal of copper ions with highly porous chitosan/cellulose acetate blend hollow fiber films, J. Membr. Sci., 284 (2006) 313–322.
[22] Z. Cheng, X. Liu, M. Han, W. Ma, Adsorption kinetic character of copper ions. onto a modified chitosan transparent thin films from aqueous solution, J. Hazard. Mater., 182 (2010) 408–415.
[23] X.C. Yan, X.P. Zhang, Q. Li, Preparation and characterization of CS/β–CD/Nano–ZnO composite porous membrane optimized by Box–Behnken for the adsorption of Congo red, Environ. Sci. Pollut. Res., 25 (2018) 22244–22258.
[24] L. Song, J. Huo, X. Wang, F. Yang, J. He, C. Li, Phosphate adsorption by a Cu (II)-loaded polyethersulfone-type metal affinity membrane with the presence of coexistent ions, Chem. Eng. J., 284 (2016) 182–193.
[25] Z.P. Zhao, Z. Wang, S.C. Wang, Formation, charged characteristic and BSA adsorption behavior of carboxymethyl chitosan/PES composite MF membrane, J. Membr. Sci., 217 (2003) 151–158.
[26] Y. Zhong, X. Song, Y. Li, Antimicrobial, physical and mechanical properties of kudzu starch–chitosan composite films as a function of acid solvent types, Carbohydr. Polym., 84 (2011) 335–342.
[27] J. Wang, Y. Liu, P. Hu, R. Huang, Adsorption of phosphate from aqueous solution by Zr (IV) crosslinked quaternized chitosan/bentonite composite, Environ. Prot. Sustainable Energy, 37 (2017) 267–275.
[28] W. Wang, B. Shan, L. Zhu, Anatase titania coated CNTs and sodium lignin sulfonate doped chitosan proton exchange membrane for DMFC application, Carbohydr. Polym., 187 (2017) 35–42.
[29] Y.Y. Su, B.L. Zhao, W. Xiao, R.P. Han, Adsorption behavior of light green anionic dye using cationic surfactant modified wheat straw in batch and column mode, Environ. Sci. Pollut. Res., 20 (2013) 5558–5568.
[30] W.L. Wang, Y.Y. Du, M.Y. Liu, M.M. Yang, R.P. Han, Adsorption of congo red from solution using chitosan modified carbon nanotubes, Desal. Water Treat., 156 (2019) 96–105.
[31] Y. Shang, J.H. Zhang, X. Wang, R.D. Zhang, W. Xiao, S.S. Zhang, R.P. Han, Use of polyethyleneimine modified wheat straw for adsorption of congo red from solution in batch mode, Desal. Water Treat., 57 (2016) 8872–8883.
[32] Y.Y. Chen, S.H. Yu, H.F. Jiang, Q.Z. Yao, S.Q. Fu, G.T. Zhou, Performance and mechanism of simultaneous removal of

Cd (II) and Congo red from aqueous solution by hierarchical vaterite spherulites, Appl. Surf. Sci., 444 (2018) 224–234.
[33] Q. Hu, N. Chen, C. Feng, Kinetic and isotherm studies of nitrate adsorption on granular Fe-Zr-chitosan complex and electrochemical reduction of nitrate from the spent regenerant solution, RSC Adv., 6 (2016) 1031–1039.
[34] M. Li, XPS study on transformation of N. and S. functional groups during pyrolysis of high sulfur New Zealand coal, J. Fuel Chem. Technol., 396 (2017) 1287–1293.
[35] S. Peng, Y. Liu, Z.Y. Xue, W.Y. Yin, X.C. Liang, M. Li, J. Chang, Modified nanoporous magnetic cellulose–chitosan microspheres for efficient removal of Pb (II) and methylene blue from aqueous solution, Cellulose, 24 (2017) 4793–4806.
[36] M. Kozlowski, XPS study of reductively and non-reductively modified coals, Fuel, 83 (2004) 259–265.
[37] Y. He, Y. Dong, L. Wan, Preferable adsorption of phosphate using lanthanum–incorporated porous zeolite: characteristics and mechanism, Appl. Surf. Sci., 426 (2017) 995–1004.
[38] R. Pietrzak, T. Grzybek, H. Wachowska, XPS study of pyrite–free coals subjected to different oxidizing agents, Fuel, 86 (2007) 2616–2624.
[39] H.K. Hen, B.Q. Li, J.L. Yang, B.J. Zhang. Transformation of sulfur during pyrolysis and hydropyrolysis of coal, Fuel, 77 (1998) 487–493.
[40] H.R. Wu, C.I. Lin, L.H. Wang, Effect of peanut hull ash dosage on the degree of influence of operation variables on the adsorption of nickel ion from aqueous solution using peanut hull ash, J. Taiwan Inst. Chem. Eng., 42 (2011) 658–661.
[41] X.N. Zhang, G.Y. Mao, Y. Shang, R.P. Han, Adsorption of anionic dye on magnesium hydroxide-coated pyrolytic bio-char and reuse by microwave irradiation, Int. J. Environ. Sci. Technol., 11 (2014) 1439–21448.
[42] R.D. Zhang, X.N. Zhang, C.C. Dou, R.P. Han, Adsorption of congo red from aqueous solutions using cationic surfactant modified wheat straw in batch mode: kinetic and equilibrium study, J. Taiwan Inst. Chem. Eng., 45 (2014) 2578–2583.
[43] Z.W. Wang, P. Han, Y.B. Jiao, X.T. He, C.C. Dou, R.P. Han, Adsorption of congo red using ethylenediamine modified wheat straw, Desal. Water Treat., 30 (2011) 195–206.
[44] T. Zhou, L.Y. Fang, X.W. Wang, M.Y. Han, S.S. Zhang, R.P. Han, Adsorption of the herbicide 2,4-dichlorophenoxyacetic acid by Fe-crosslinked chitosan complex in batch mode, Desal. Water Treat., 70 (2017) 294–301.
[45] T. Feng, F. Zhang, J. Wang, Application of chitosan-coated quartz sand for Congo red adsorption from aqueous solution, J. Appl. Polym. Sci., 125 (2012) 1766–1772.
[46] J.J. Chen, X.W. Shi, Y.F. Zhan, X.D. Qiu, Y.M. Du, H.B. Deng, Construction of horizontal stratum landform–like composite foams and their methyl orange adsorption capacity, Appl. Surf. Sci., 397 (2017) 133–2143.
[47] Y.C. Rong, H. Li, L.H. Xiao, Q. Wang, Y.Y. Hu, S.S. Zhang, R.P. Han, Adsorption of malachite green dye from solution by magnetic-activated carbon in batch mode, Desal. Water Treat., 106 (2018) 273–284.
[48] H.M. Zhu, M.M. Zhang, Y.Q. Liu, L.J. Zhang, R.P. Han, Study of congo red adsorption onto chitosan coated magnetic iron oxide in batch mode, Desal. Water Treat., 37 (2012) 46–54.
[49] J.Y. Song, W.H. Zou, Y.Y. Bian, F.Y. Su, R.P. Han, Adsorption characteristics of methylene blue by peanut husk in batch and column mode, Desalination, 265 (2011) 119–2125.
[50] F. Gunduz, B. Bayrak, Biosorption of malachite green from an aqueous solution using pomegranate peel: equilibrium modeling, kinetic and thermodynamic studies, J. Mol. Liq., 243 (2017) 790–798.
[51] M.I. Konggidinata, B. Chao, Q.Y. Lian, R. Subramaniam, M. Zappi, D.D. Gang, Equilibrium, kinetic and thermodynamic studies for adsorption of BTEX onto ordered mesoporous carbon (OMC), J. Hazard. Mater., 336 (2017) 249–259.
[52] T. Maneerung, J. Liew, Y. Dai, S. Kawi, C. Chong, C.H. Wang, Activated carbon derived from carbon residue from biomass gasification and its application for dye adsorption: kinetics, isotherms and thermodynamic studies, Bioresour. Technol., 200 (2016) 350–359.
[53] Y.Y. Hu, R.P. Han, Selective and efficient removal of anionic dyes from solution by zirconium (IV) hydroxide coated magnetic materials, J. Chem. Eng. Data, 64 (2019) 791–799.
[54] J.W. Fu, Z.H. Chen, M.H. Wang, S.J. Liu, J.H. Zhang, J.N. Zhang, R.P. Han, Q. Xu, Adsorption of methylene blue by a high-efficiency adsorbent (polydopamine microspheres): kinetics, isotherm, thermodynamics and mechanism analysis, Chem. Eng. J., 259 (2015) 53–61.
[55] W. Konicki, M. Aleksandrzak, D. Moszyński, E. Mijowska, Adsorption of anionic azo-dyes from aqueous solutions onto graphene oxide: equilibrium, kinetic and thermodynamic studies, J. Colloid Interface Sci., 496 (2017) 188–200.
[56] M.Y. Han, Q. Wang, H. Li, L.Y. Fang, R.P. Han, Removal of methyl orange from aqueous solutions by polydopamine mediated surface functionalization of Fe_3O_4 in batch mode, Desal. Water Treat., 115 (2018) 271–280.
[57] T. Zhou, W.Z. Lu, L.F. Liu, H.M. Zhu, Y.B. Jiao, S.S. Zhang, R.P. Han, Effective adsorption of light green anionic dye from solution by CPB modified peanut in column mode, J. Mol. Liq., 211 (2015) 909–2914.
[58] S. Sadaf, H.N. Bhatti, Evaluation of peanut husk as a novel, low-cost biosorbent for the removal of Indosol Orange RSN dye from aqueous solutions: batch and fixed bed studies, Clean Technol. Environ., 16 (2014) 527–544.
[59] B.L. Zhao, W. Xiao, Y. Shang, H.M. Zhu, R.P. Han, Adsorption of light green anionic dye using cationic surfactant-modified peanut husk in batch mode, Arabian J. Chem., 10 (2017) S3595–S3602.
[60] J. Xu, D.F. Xu, B.C. Zhu, B. Cheng, C.J. Jiang, Adsorptive removal of an anionic dye Congo red by flower-like hierarchical magnesium oxide (MgO)-graphene oxide composite microspheres, Appl. Surf. Sci., 435 (2018) 1136–1142.